Proceedings of the 25th International Conference on
Port and Ocean Engineering under Arctic Conditions
June 9-13, 2019, Delft, The Netherlands

Statistical analysis of ice-induced loads on the Norströmsgrund lighthouse

Ying Tu[1], Torodd S. Nord[2,3], Knut V. Høyland[2], Øyvind Wiig Petersen[4]
[1] Department of Civil and Environmental Engineering, Norwegian University of Science and Technology, Trondheim, Norway
[2] Sustainable Arctic Marine and Coastal Technology (SAMCoT), Centre for Research-based Innovation (CRI), Norwegian University of Science and Technology, Trondheim, Norway
[3] The University Centre in Svalbard (UNIS), Longyearbyen, Spitsbergen, Norway
[4]Department of Structural Engineering, Norwegian University of Science and Technology, Trondheim, Norway

ABSTRACT

Structures may experience ice-induced vibrations under a wide range of ice conditions. This paper presents a statistical analysis of ice-induced forces on the Norströmsgrund lighthouse. A total of 61 measured events of ice-induced frequency lock-in (FLI) vibrations from 2001 until 2003 are considered. For each event, a smoothing algorithm for joint input-state (JIS) estimation is used to identify the time series of ice-induced dynamic forces based on measured accelerations. The smoothing algorithm is validated by comparing the identified dynamic force with the measured dynamic force. Statistical analysis on these 61 events indicates that the identified force directions agree well with the observed ice-drift directions. However, a universal relation between peak force and ice thickness or ice velocity is not found. Significant peak forces are likely to occur under ice conditions with ice thickness between 0.65m and 0.85m and ice velocity ranging from 0.042m/s and 0.05m/s.

KEY WORDS: Ice-induced vibration; Joint input-state estimation; Frequency lock-in; Norströmsgrund lighthouse.

INTRODUCTION

Offshore structures exposed to drifting ice may experience ice-induced vibration, which can cause fatigue damage and affect structural integrity. Due to ice-induced vibration, the KEMI-1 steel lighthouse collapsed only some months after its deployment in the Gulf of Bothnia (Määttänen, 1975). According to ISO (2010), ice-induced vibration can be classified into three regimes: intermittent crushing, frequency lock-in (FLI) and continuous brittle crushing. These three regimes correspond to level ice interacting with an offshore structure at low, mediate and high ice speeds, respectively (Yue et al., 2009). Among them, the FLI regime is most violent and can cause sinusoidal structural responses when the ice failure frequency is locked at one of the lowest modes of the structure (ISO, 2010). This definition was debated in

Nord et al. (2018), as many recordings of high-amplitude ice-induced vibrations that were measured on the Norströmsgrund lighthouse had non-stationary response amplitudes, thus, they were not sinusoidal.

FLI has been measured on many offshore bottom-fixed structures, such as lighthouses (Määttänen, 1975; Määttänen, 2008; Nord et al., 2018) and jacket structures (Yue and Bi, 2000). It is characterized by high amplitude oscillations near a natural frequency.

Based on the 61 events of ice-induced vibrations identified by Nord et al. (2018), this study presents a statistical analysis of ice-induced forces on the Norströmsgrund lighthouse. A smoothing algorithm for joint input-state (JIS) estimation is used to identify the ice-induced forces for each event based on measured accelerations in conjunction with a finite element model. The algorithm yields more accurate results than the traditional JIS (Lourens et al. 2012, Nord et al. 2015) when accelerations are non-collocated, and due to the smoothing, a stable inversion is obtained. After the time series of the ice-induced forces of the 61 events are identified, a statistical analysis is carried out to reveal the statistical characteristics between the forces and the ice conditions, i.e. ice thickness and ice velocity.

DATA DESCRIPTION

The data used for the analysis were acquired in a full-scale measurement campaign on the Norströmsgrund lighthouse in the time period 2001–2003 (Nord et al., 2018). As illustrated in Figure 1, the location of the lighthouse is 65°6.6'N and 22°19.3'E, where landfast ice prevails nearby along the coast area of Luleå, Sweden, and drifting ice zone exists in the Gulf of Bothnia. The dominant annual peak level ice thickness falls in the range of 0.6 to 0.8m. The water depth varies around 13m. The diameter of the lighthouse is 7.52m at the waterline (Li, 2015).

Figure 1. Location of the Norströmsgrund lighthouse (Li, 2015)

Two accelerometers were installed at +16.5m and +37.1m above the bottom of the structure, respectively, as shown in Figure 2(a). Each accelerometer measured accelerations in two directions in the horizontal plane, North-South (NS) and East-West (EW). They are used to

identify the global dynamic forces due to ice-structure interactions in this study. The coordinate system for the acceleration measurement and ice force is defined in Figure 2(c). The direction towards south is defined as positive x, while the direction towards west is defined as positive y. The channels of acceleration measurements are given in Table 1.

In addition, nine force panels measured local ice forces at the Mean Water Level (MWL) as shown in Figure 2(a). They covered 162° of the outer perimeter from the North to the Southeast (Frederking, 2003), as shown in Figure 2(b). The total dynamic ice forces can be estimated from the panel measurements and they are used to validate the identified dynamic forces based on acceleration measurements in the present study.

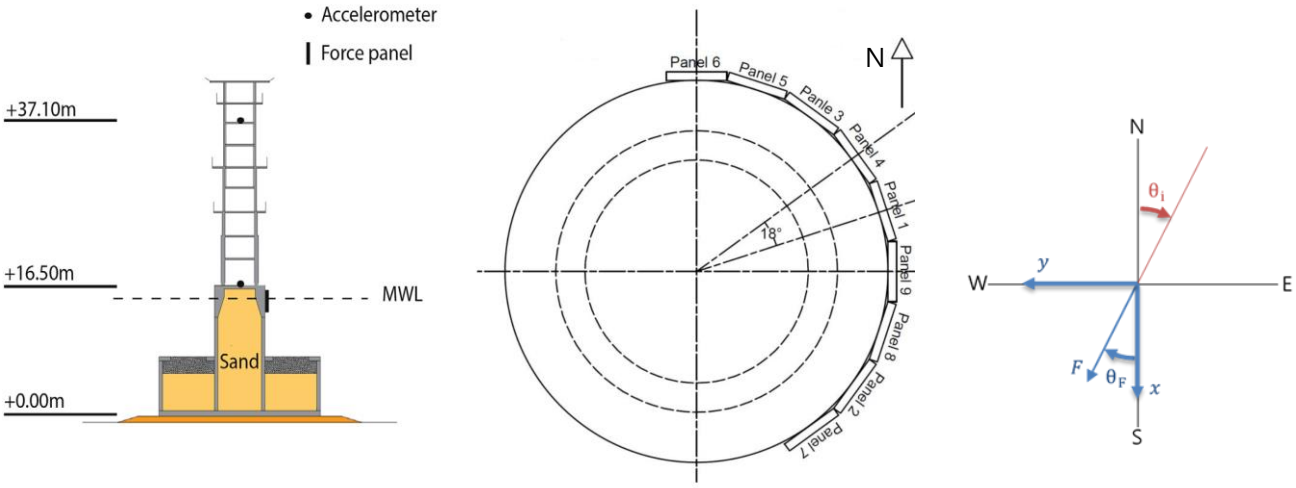

(a) (b) (c)

Figure 2. (a) Locations of the accelerometers and force panels (Nord et al., 2018); (b) coverage of the force panels over the outer perimeter (Frederking, 2003); (c) definition of coordinate system, force direction θ_F and ice-drift direction θ_i (where ice comes from)

Table 1. Acceleration channels

Acceleration channel	Height [m]	Direction	Positive
1	16.50	North-south (NS)	Towards south
2	16.50	East-West (EW)	Towards west
3	37.10	North-south (NS)	Towards south
4	37.10	East-West (EW)	Towards west

According to the definition and criteria in Nord et al. (2018), 61 events that we argue to be classified as FLI vibrations are selected. These events and the corresponding ice-drift direction from observation, ice thickness and ice-drift velocity from measurements, are given in Table A in the appendix. The ice-drift direction, as shown in Figure 2(c), is defined as the coming direction of the ice, and it is counted clockwise from 0° in the North. The measured acceleration time series of an FLI event is illustrated in Figure 3.

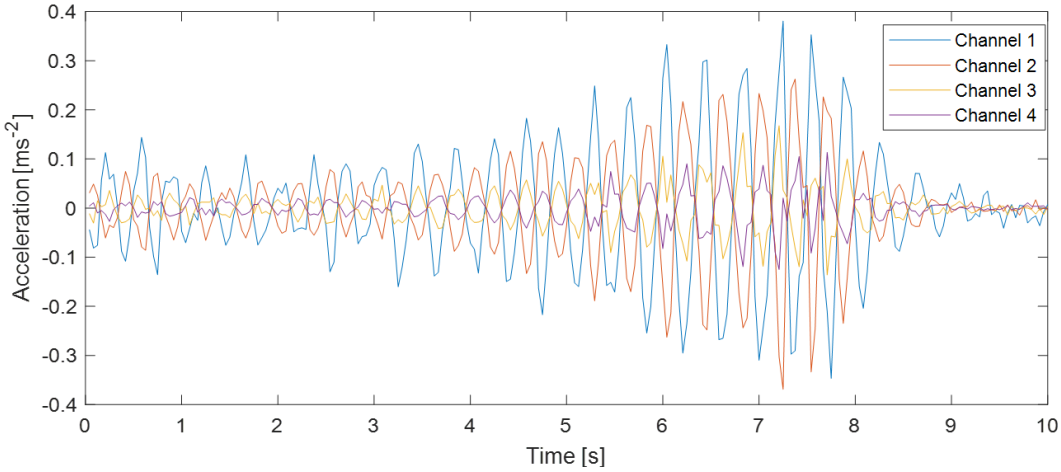

Figure 3. Measured acceleration time series of Event 3

The sampling frequency varies significantly among different events, as shown in Figure 4. The mean sampling frequency ranges from about 10Hz to about 86Hz, and for the majority of the event, the value is 30Hz. On the contrary, the variation of sampling frequency within each event is hardly noticeable. The coefficients of variation (CoV) of the sampling frequency for each event are all smaller than 0.004. This slight variation may be caused by the rounding errors in the logging system of the experiment.

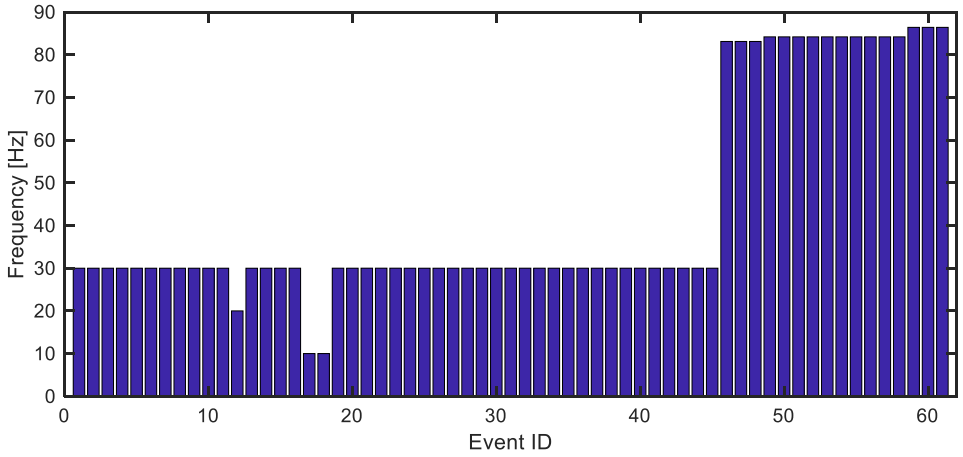

Figure 4. Mean value of sampling frequency for each event

METHODS

Pre-processing

The calculated total forces from the force panel measurements have both a dynamic part and a slowly varying quasi-static part. A high pass filter is first applied to eliminate the quasi-static part, so that the remaining dynamic part can be compared to the identified dynamic force. Moreover, since most of the events have a sampling frequency of around 30Hz, the time series of the measurements of all events are resampled to 30Hz. The effect of resampling of the acceleration time series can be seen from Figure 5.

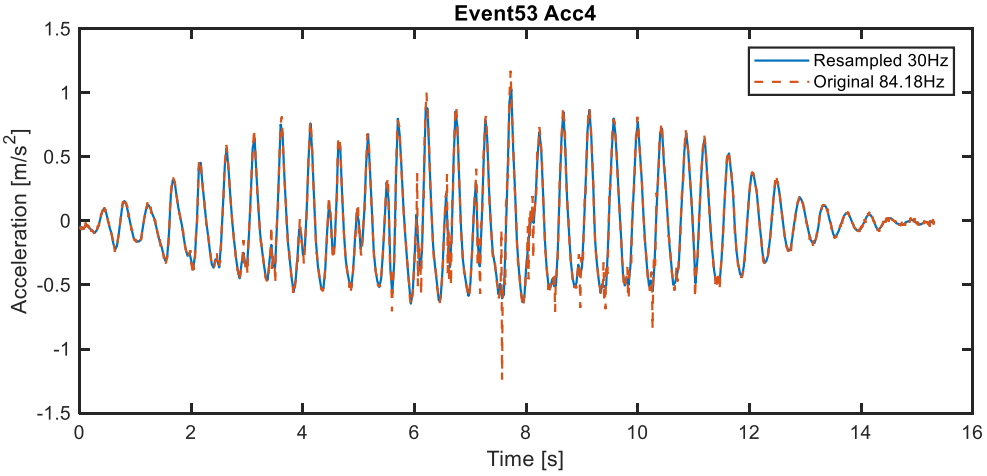

Figure 5. Resampling of measured acceleration for event 53 and channel 4

In addition, the acceleration measurements may have an opposite sign to the real values in some channels for some events. These channels have been adjusted before the acceleration data is used for the identification of dynamic forces. For the events in which the order of the measurement channels was swapped, the order is changed to follow the definition given in Table 1.

Force identification

Since the force panels shown in Figure 2 only covers 45% percent of the outer perimeter, they cannot capture the ice-induced dynamic forces from all ice-drift directions. These can, however, be identified from acceleration measurements and the joint input-state (JIS) estimation algorithm.

In the JIS estimation, the state space model of the structure is generated by a finite element model in Nord et al. (2016). The smoothing algorithm by Maes et al. (2018) is applied, in which a time delay is considered in the JIS estimation. To obtain a stable estimation process, indirect displacement measurements are also generated from numerical integration of the accelerations. The pre-processed response measurement data are fed into the algorithm to identify the ice-induced dynamic forces on the structure. In this study, a time delay of L=10 (i.e., 10 time steps) is used in the smoothing algorithm.

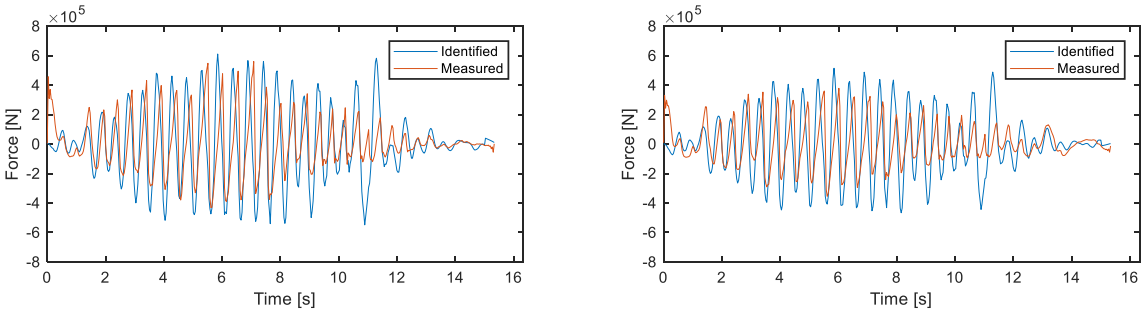

(a) Force in EW direction (b) Force in NS direction

Figure 6. Comparison of identified and measured dynamic forces in EW and NS directions for event 53

The identified forces are validated by comparison against the filtered total forces that were calculated from the force measurement, especially for those events where ice drifted towards the walls covered with the force panels. Figure 6 illustrates the comparison for Event 53. The

ice-drift direction is 45° for this event, which implies that the total forces are mostly captured by the force panels. The identified and the measured forces have a good agreement in this event, but the identified forces have slightly larger amplitudes. This implies that the implemented smoothing algorithm can provide a good identification result of the dynamic forces.

RESULTS AND DISCUSSION

Resultant force and force direction

The magnitude and the direction of the resultant force can be estimated from the identified force components, i.e., F_x in the NS direction and F_y in the EW direction, as follows

$$F = \sqrt{F_x^2 + F_y^2} \tag{1}$$

$$\theta_F = \arctan(\frac{F_y}{F_x}) \tag{2}$$

Therefore, the direction of the resultant force θ_F is counted clockwise from 0° in the south, as shown in Figure 2(c).

In order to compare the identified force directions to the ice-drift directions, polar histograms of the force directions are plotted for each event. Figure 7 shows some representative results of the comparison. For all the events, the forces are in two dominate directions opposite to each other, because only the dynamic forces are taken into count, and their values fluctuate around zero. For most events, the force directions and the ice-drift directions are aligned. In Event 7, however, the major force direction is about 330°, while the ice-drift direction is 270°. This misalignment can be explained by misreport of the ice-drift direction, after the video of the event is checked.

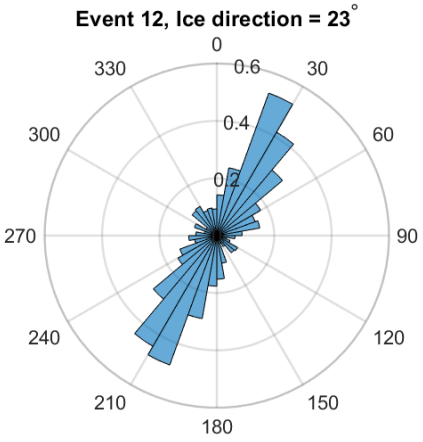

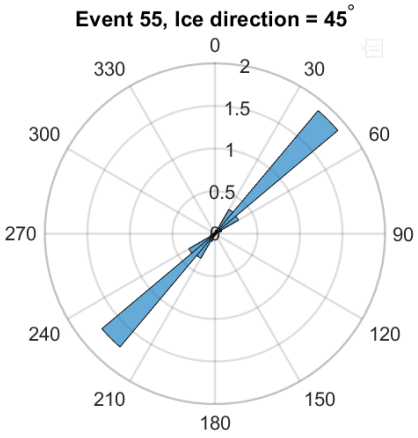

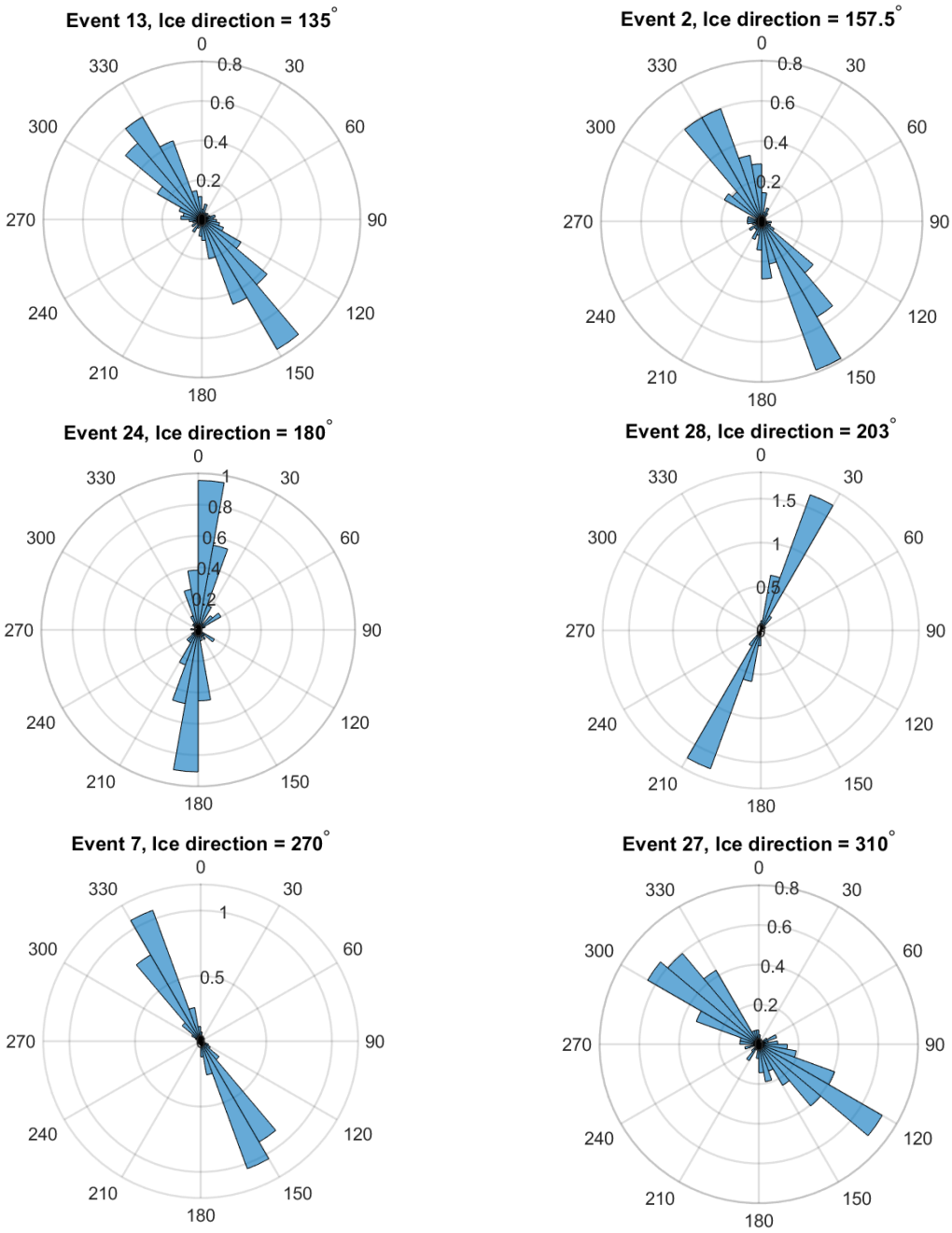

Figure 7. Probability density distribution of the direction of identified resultant force for several selected events. The observed ice-drift direction is also given for each event

Peak force and average of top 10% peak forces

The peak force is of interest from practical design point of view. For each event, the peaks of the resultant force time series are first extracted. Since only considering the largest peak might introduce significant uncertainty, the average of the top 10% peaks is also introduced and presented here. The top 10% peaks can be obtained from the time series. Accordingly, the average and the coefficient of variation (CoV) of the top 10% peaks can be estimated. Figure 8 shows an example of the time series of the resultant force for event 53, the peaks, largest peak and top 10% peaks are marked in the figure. The calculated largest peak, average and CoV of top 10% peaks for each event are given in Table A in the appendix.

To characterize the variation of high peaks, the CoV of top 10% peaks and the ratio of the average of the top 10% peaks to the largest peak, denoted by $F_{P,1/10}/F_P$, for each event are

plotted in Figure 9. A smaller CoV generally corresponds to a relatively large value of $F_{P,1/10}/F_P$. In all 61 events, 53 events have a CoV of top 10% peaks smaller than 0.2. In addition, the CoV of top 10% peaks is smaller than 0.3 for all events, except event 42. The CoV for event 42 reaches 0.435, because it has a significant largest peak. Because the CoV of top 10% peaks is relatively small for all events considered, the average of top 10% peaks is thus considered as the representative value for characteristic peak force.

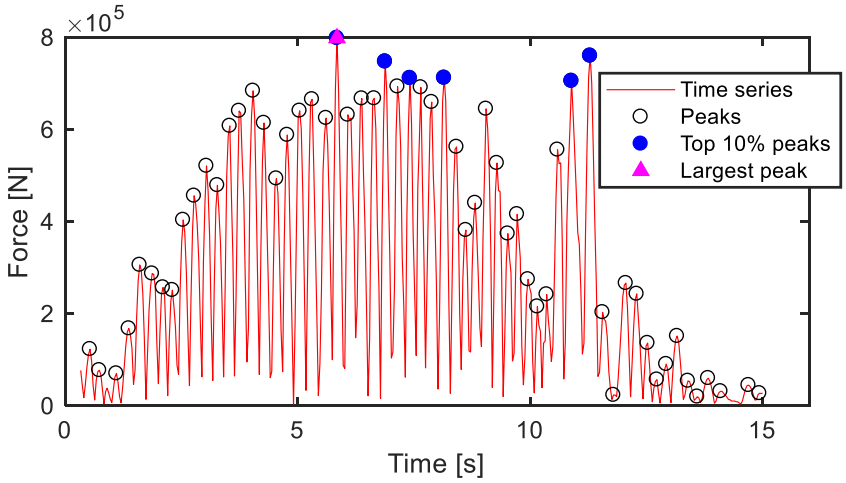

Figure 8. Time series of the magnitude of the resultant force for event 53. The peak forces and top 10% peaks are marked in the time series

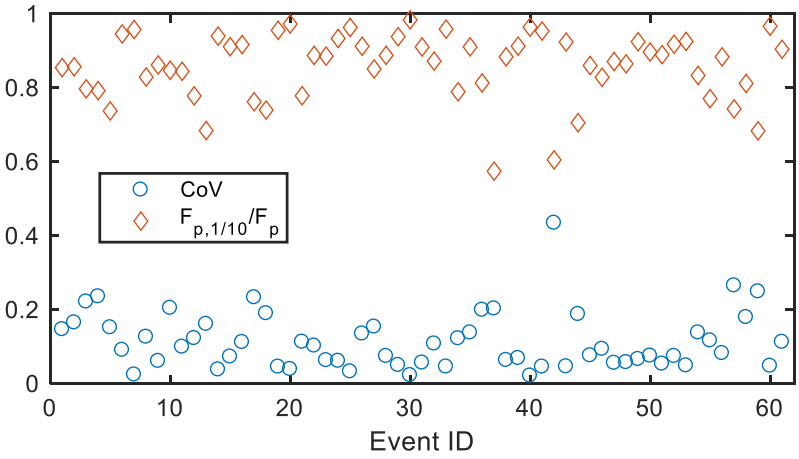

Figure 9. Coefficient of variation (CoV) of the top 10% peaks, and the ratio of average of the top 10% peaks to the largest peak $F_{P,1/10}/F_P$ for each event

Relation between peak force and ice conditions

In this section, the relation between resultant force magnitude and ice conditions, i.e. ice thickness and ice-drift velocity, is studied statistically. The resultant force due to ice-induced vibration is represented by peak forces. Both the largest peak F_P and the average of top 10% peaks $F_{P,1/10}$ discussed in the above section are considered here. For each event, the ice conditions including ice thickness and ice velocity were recorded by field measurements. The values of largest peak, average of top 10% peaks, ice thickness and ice velocity for each event are given in Table A in the appendix.

Figure 10 shows the scatter plots of peak force vs. ice thickness, and peak force vs. ice velocity. For most events, the ice thickness ranges from 0.6m to 1m, ice velocity ranges from

0.028m/s to 0.059m/s. The peak force represented by $F_{P,1/10}$ has a smaller variation than that denoted by F_P. However, a universal relation between peak force and ice thickness or ice velocity can not be found.

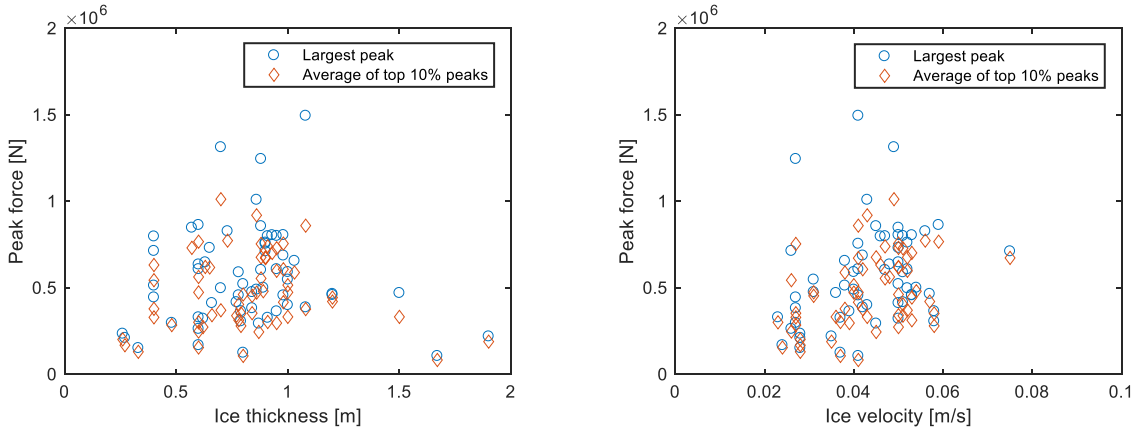

(a) Peak force vs. ice thickness (b) Peak force vs. ice velocity

Figure 10. Scatter plot of (a) peak force vs. ice thickness, and (b) peak force vs. ice velocity for each event. The peak force is represented by the largest peak and the average of top 10% peaks, respectively

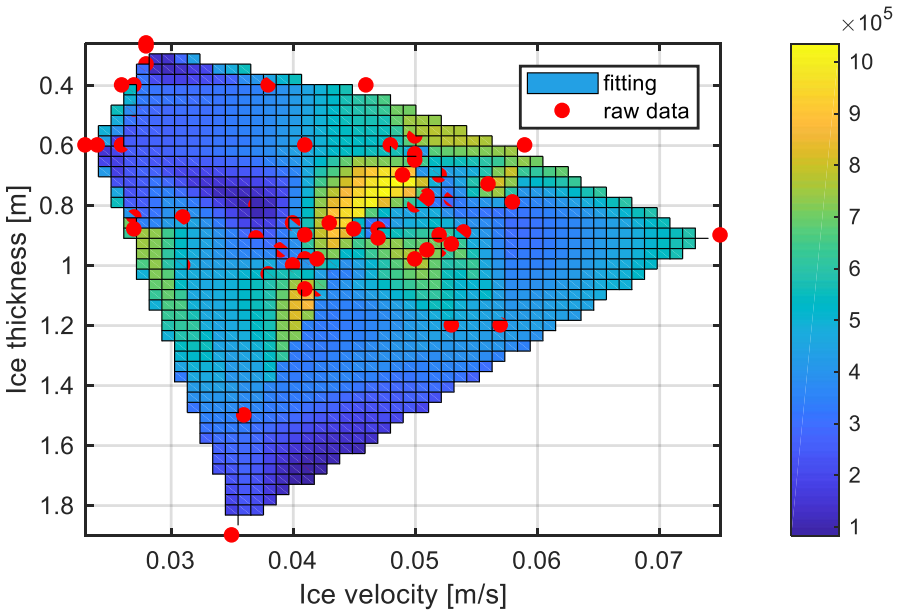

Figure 11. Relation between average of the top 10% peaks, and ice thickness and velocity

Figure 11 shows the relation between the average of top 10% peaks, ice thickness and ice velocity. It can be observed that significant peak forces correspond to ice thickness between 0.65m and 0.85m and ice velocity ranging from 0.042m/s to 0.05m/s.

It is common to normalize the parameters on the axes of Figure 10 and 11 for a clearer interpretation of the results. However, since we only have the results from one structure with a constant diameter, such normalization does not provide us with more information and is therefore not carried out.

CONCLUSIONS

This study comprehends a statistical analysis of ice-induced dynamic forces on the Norströmsgrund lighthouse based on 61 measured events of resonant vibrations. For each event, a smoothing algorithm for joint input-state estimation is used to identify the ice-induced forces based on measured accelerations. Main conclusions are as follows:

- The smoothing algorithm for joint input-state estimation can provide a good identification of time series of ice-induced force.
- The identified dynamic force directions agree well with the corresponding observed ice-drift directions.
- The average of top 10% peaks of resultant force is a representative value for characteristic peak force, compared to the largest peak.
- A universal relation between peak force and ice thickness or ice velocity cannot be found.
- Significant dynamic peak forces are likely to occur under ice conditions with ice thickness between 0.65m and 0.85m and ice velocity ranging from 0.042m/s to 0.05m/s.
-

ACKNOWLEDGEMENT

This work has been supported by MarTERA partners Research Council of Norway (RCN) and German Federal Ministry of Economic Affairs and Energy (BMWi) and co-funded by the European Union in the framework of FATICE project.

APPENDIX

Table A. Events of resonant vibration measured between 2001 and 2003

Event ID	Date of event	Data file id	Start time	End time	Ice direction	Ice thickness	Ice velocity	Largest Peak	Average of top 10% peak	CoV of top 10% peak
		[DD.MM.YYYY]	[hhmmss]	[hhmmss]	deg	[m]	[m/s]	[10^5N]	[10^5N]	
1	28.03.2001	01_2803_0300	81123	81132	157.5	0.33	0.028	1.52	1.30	0.15
2	28.03.2001	01_2803_0300	84230	84237	157.5	0.26	0.028	2.35	2.01	0.17
3	28.03.2001	01_2803_0300	90538	90547	157.5	0.27	0.028	2.11	1.68	0.22
4	01.04.2001	01_0104_0400	93357	93405	202.5	0.4	0.046	7.97	6.32	0.24
5	01.04.2001	01_0104_0400	93847	93927	202.5	0.4	0.038	5.13	3.78	0.15
6	05.04.2001	01_0504_0400	154755	154802	135	0.9	0.075	7.11	6.73	0.09
7	09.04.2001	01_0904_0400	223741	223807	270	0.63	0.05	6.48	6.20	0.02
8	09.04.2001	01_0904_0400	223830	223845	270	0.66	0.05	4.12	3.42	0.13
9	09.04.2001	01_0904_0400	223920	223953	270	0.57	0.05	8.48	7.31	0.06
10	09.04.2001	01_0904_0400	224012	224023	270	0.62	0.05	3.22	2.73	0.21
11	09.04.2001	01_0904_0400	224157	224233	270	0.65	0.05	7.31	6.18	0.10
12	27.02.2002	02_2702_0200	191534	191612	23	1.67	0.041	1.06	0.83	0.12
13	06.03.2002	02_0603_0100	2310	2345	135	0.78	0.051	5.90	4.04	0.16
14	19.03.2002	02_1903_0700	215818	215830	150	0.6	0.026	2.63	2.47	0.04
15	19.03.2002	02_1903_0700	220044	220102	150	0.6	0.023	3.30	3.01	0.07
16	19.03.2002	02_1903_0700	220600	220610	150	0.6	0.024	1.69	1.55	0.11
17	02.04.2002	02_0204_0200	64842	64856	180	0.4	0.026	7.14	5.44	0.23
18	04.04.2002	02_0404_0200	103826	103847	135	0.4	0.027	4.45	3.29	0.19
19	04.04.2002	02_0404_0300	104315	104323	135	0.48	0.027	2.98	2.84	0.05
20	07.04.2002	02_0704_0200	54040	54046	23	1.08	0.042	3.87	3.77	0.04
21	09.03.2003	03_0903_0200	5607	5640	220	0.6	0.041	6.08	4.74	0.11
22	09.03.2003	03_0903_0200	10023	10040	220	0.6	0.059	8.64	7.67	0.10
23	09.03.2003	03_0903_0200	10340	10401	220	0.6	0.048	6.35	5.63	0.06
24	10.03.2003	03_1003_0200	35915	35922	180	0.73	0.056	8.28	7.73	0.06
25	10.03.2003	03_1003_0200	40112	40118	180	0.79	0.058	3.65	3.52	0.03
26	10.03.2003	03_1003_0200	40136	40142	180	0.79	0.058	3.07	2.80	0.14
27	14.03.2003	03_1403_0400	221620	221627	310	0.8	0.037	1.25	1.06	0.15
28	25.03.2003	03_2503_0600	153247	153258	203	0.9	0.052	7.62	6.76	0.07
29	25.03.2003	03_2503_0600	153343	153403	203	0.98	0.05	8.05	7.56	0.05

30	25.03.2003	03_2503_0600	153617	153623	203	0.95	0.052	6.08	5.98	0.02
31	25.03.2003	03_2503_0600	153640	153653	203	0.95	0.051	8.00	7.29	0.06
32	25.03.2003	03_2503_0600	153708	153722	203	0.93	0.053	8.05	7.02	0.11
33	25.03.2003	03_2503_0600	154318	154327	203	0.89	0.054	5.01	4.80	0.05
34	25.03.2003	03_2503_0600	155658	155743	203	0.88	0.045	8.57	6.76	0.12
35	25.03.2003	03_2503_0600	160101	160105	180	0.86	0.043	10.09	9.19	0.14
36	25.03.2003	03_2503_0600	160234	160240	180	0.95	0.039	3.64	2.96	0.20
37	25.03.2003	03_2503_0600	160632	160751	180	1.08	0.041	14.95	8.59	0.20
38	25.03.2003	03_2503_0600	162054	162139	180	0.98	0.042	6.87	6.07	0.06
39	25.03.2003	03_2503_0600	162255	162305	180	0.98	0.041	4.56	4.17	0.07
40	25.03.2003	03_2503_0600	163159	163212	180	0.86	0.04	4.90	4.72	0.02
41	25.03.2003	03_2503_0600	170523	170530	180	0.84	0.031	4.76	4.53	0.05
42	25.03.2003	03_2503_0600	171120	171130	180	0.88	0.027	12.45	7.54	0.44
43	25.03.2003	03_2503_0600	171242	171253	180	0.84	0.027	3.82	3.53	0.05
44	25.03.2003	03_2503_0700	192148	192320	180	1.5	0.036	4.70	3.32	0.19
45	25.03.2003	03_2503_0700	192448	192514	180	1.9	0.035	2.19	1.89	0.08
46	26.03.2003	03_2603_0200	121746	121825	180	1	0.043	4.00	3.32	0.09
47	26.03.2003	03_2603_0200	122829	122955	180	1	0.04	5.92	5.15	0.06
48	26.03.2003	03_2603_0200	123118	123218	180	1	0.031	5.48	4.74	0.06
49	30.03.2003	03_3003_0400	120338	120352	45	0.91	0.037	3.27	3.02	0.07
50	30.03.2003	03_3003_0400	120524	120539	45	1.03	0.038	6.56	5.88	0.08
51	30.03.2003	03_3003_0400	120547	120624	45	0.9	0.041	7.55	6.72	0.05
52	30.03.2003	03_3003_0400	121419	121431	45	0.88	0.047	6.03	5.54	0.07
53	30.03.2003	03_3003_0400	121500	121514	45	0.91	0.047	7.99	7.39	0.05
54	30.03.2003	03_3003_0400	121738	121748	45	0.87	0.045	2.94	2.45	0.14
55	30.03.2003	03_3003_0400	122538	122700	45	0.7	0.049	13.13	10.12	0.12
56	30.03.2003	03_3003_0400	122950	123007	45	0.8	0.05	5.22	4.61	0.08
57	30.03.2003	03_3003_0400	123301	123311	45	0.7	0.052	4.98	3.70	0.27
58	30.03.2003	03_3003_0400	124243	124253	45	0.77	0.051	4.17	3.39	0.18
59	30.03.2003	03_3003_0500	125818	125847	45	0.78	0.053	4.57	3.12	0.25
60	30.03.2003	03_3003_0500	130144	130148	45	1.2	0.053	4.59	4.43	0.05
61	30.03.2003	03_3003_0500	130918	130928	45	1.2	0.057	4.65	4.21	0.11

REFERENCES

Frederking, R.M.W., 2003. *STRICE Project: Tiltmeter Application on Norstromsgrund Lighthouse*, National Research Council Canada, Canadian Hydraulics Centre.

ISO, 2010. ISO/FDIS 19906. pp. 188.

Li, H., 2015. *Measurement Setup at Lighthouse Norströmsgrund and Data Processing 1999 – 2003*, Department of Civil and Transport Engineering, NTNU, Trondheim.

Lourens, E., Papadimitriou, C., Gillijns, S., Reynders, E., De Roeck, G. and Lombaert, G., 2012. Joint input-response estimation for structural systems based on reduced-order models and vibration data from a limited number of sensors. *Mechanical Systems and Signal Processing*, 29, pp.310-327.

Maes, K., Gillijns, S. and Lombaert, G., 2018. A smoothing algorithm for joint input-state estimation in structural dynamics. *Mechanical Systems and Signal Processing*, 98, pp.292-309.

Määttänen, M., 1975. Experiences of Ice Forces against a Steel Lighthouse Mounted on the Seabed, and Proposed Constructional Refinements, Port and Ocean Engineering under Arctic Conditions (POAC). Fairbanks, Alaska, pp. 857–867.

Määttänen, M., 2008. Ice Velocity Limit to Frequency Lock-in Vibrations. International symposium on Ice, IAHR, Vancouver, Canada, pp. 1265–1276.

Nord, T.S., Øiseth, O. and Lourens, E.M., 2016. Ice force identification on the Nordströmsgrund lighthouse. *Computers & Structures*, 169, pp.24-39.

Nord, T.S., Samardžija, I., Hendrikse, H., Bjerkås, M., Høyland, K.V. and Li, H., 2018. Ice-induced vibrations of the Norströmsgrund lighthouse. *Cold Reg. Sci. Technol.*, 155, pp.237-251.

Yue, Q., Bi, X., 2000. Ice-induced jacket structure vibrations in Bohai Sea. *J. Cold Reg. Eng.* 14 (2), 81–92.

Yue, Q., Guo, F., Kärnä, T., 2009. Dynamic ice forces of slender vertical structures due to ice crushing. *Cold Reg. Sci. Technol.* 56 (2–3), 77–83.